6

A Novel Compact Photonic Crystal Fibre Surface Plasmon Resonance Biosensor for an Aqueous Environment

Emmanuel K. Akowuah, Terry Gorman, Huseyin Ademgil, Shyqyri Haxha, Gary Robinson and Jenny Oliver
University of Kent, Canterbury
United Kingdom

1. Introduction

Surface plasmon resonance (SPR) sensors provide high sensitivity without the use of molecular labels (Homola, Yee, and Gauglitz 1999). They been widely used in the analysis of biomolecular interactions (BIA) and detection of chemical and biological analytes (Homola, Yee, and Gauglitz 1999), where they provide benefits of real-time, sensitive and label-free technology. They have also been used for the detection of various chemical and biological compounds in areas such as environmental protection, food safety and medical diagnostics (Mouvet et al. 1997; Nooke et al. 2010).

Most commercial SPR biosensors are based on the simple, robust and highly sensitive traditional prism-coupled configuration. However, they are not amenable to miniaturization and integration (Jha and Sharma 2009). There is therefore a growing interest in the development of robust, portable and highly sensitive SPR sensing devices capable of out of laboratory measurements (Akowuah et al. 2010; Piliarik et al. 2009; Wang et al. 2010).

Several compact configurations, enabling coupling between optical waveguide modes and surface plasmon waves have been investigated over the last decade. Among these inlcude metalized single-mode, polarization maintaining, and multimode waveguides, metalized tapered fibers, metalized fiber Bragg gratings and lapped D-shaped fiber sensors have been studied(Jorgenson and Yee 1993; Monzon-Hernandez and Villatoro 2006). Fibre optic SPR biosensors offer miniaturization, a high degree of integration, and remote sensing capabilities (Patskovsky et al. 2010; Hoa, Kirk, and Tabrizian 2007).

There is currently interest in the design of photonic crystal fibre (PCF) SPR sensors, which are based on the coupling of a leaky core mode to the SPP mode along a metalized fiber micro-structure (Dhawan, Gerhold, and Muth 2008). This has resulted in the proposal of many types of PCF and micro structured optical fiber (MOF) SPR biosensors, some of which include a three-hole MOF SPR biosensor with a gold layer deposited on the holes, PCF SPR biosensor with enhanced micro fluids and photonic bandgap SPR biosensors (Gauvreau et al. 2007; Hassani et al. 2008; Hassani and Skorobogatiy 2006; Hautakorpi, Mattinen, and Ludvigsen 2008). PCFs are thin silica glass fibers possessing a regular array of microscopic

holes that extend along the whole fiber length (Ferrando et al. 2000). The discovery of PCFs has led to several possibilities, ranging from guidance of light in vacuum, to achieving unusual dispersion properties, from enhancing non-linear effects to high confinement of light and minimizing the same non-linear effects through very large mode area single mode fibers (Ademgil et al. 2009). These unusual properties of PCFs have led to an increasing interest in their application in areas such as sensing, signal processing and optical communication systems (Ferrando et al. 2000; Ademgil et al. 2009).

This chapter presents the numerical analysis of a novel sensitive PCF SPR biosensor optimised for operation in aqueous environments. The proposed sensor, shown in Fig. 1, consists of two metalized micro fluidic slots, air holes for light guidance and a small central air hole to facilitate phase matching between guided and plasmon modes. The proposed PCF SPR sensor incorporates extra air holes between the main air holes as a means of reducing the propagation losses whilst ensuring efficient coupling between the core guided and plasma modes.

It will be shown that the proposed PCF SPR sensor can be optimised to achieve a sensitivity of 4000 nm/RIU with regards to spectral interrogation, which is much higher than the 1000 nm/RIU and 3000 nm/RIU reported by (Hautakorpi, Mattinen, and Ludvigsen 2008) and (Hassani and Skorobogatiy 2006) respectively.

With regards to fabrication, the proposed structure should be relatively easy to fabricate due to the notably large micro fluidic slots. Deposition of metal layers inside of the micro fluidic slots can be performed either with the high-pressure chemical vapour deposition technique (Sazio 2006) or electroless plating techniques used in fabrication of metalized hollow waveguides and microstructures (Harrington 2000; Takeyasu, Tanaka, and Kawata 2005).

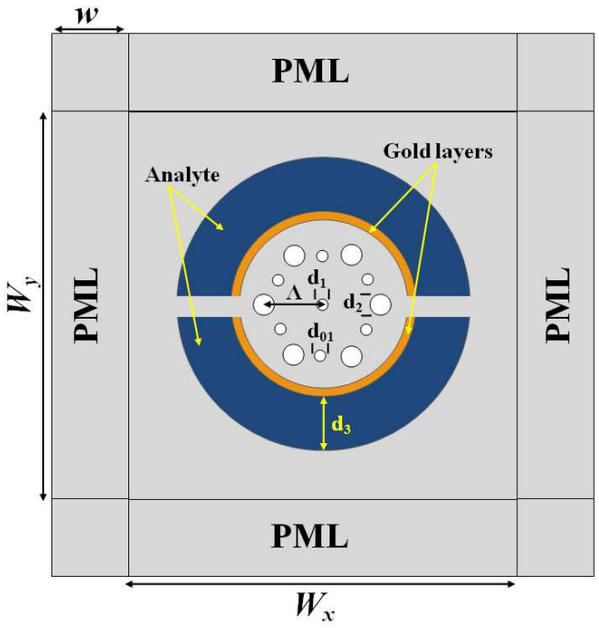

Fig. 1. Cross section of the proposed PCF SPR biosensor showing various sections.

A full – vectorial Finite Element Method (FEM) with perfectly matched layers (PML) is employed to investigate the variation of key performance parameters such as sensitivity and

confinement losses with structural parameters such as air hole diameter and gold thickness in the next section of the chapter, followed by conclusion in the final section.

2. Full Vectorial FEM

The finite element method (FEM) can be applied to waveguides in general and PCFs in particular to investigate propagation characteristics of modes. In the case of PCFs, the fibre cross section is divided into homogeneous subspaces where Maxwell's equations are solved by accounting for the adjacent subspaces. These subspaces are triangles which give good approximation of circular structures (Saitoh and Koshiba 2001).

In order to allow the study of fibers with arbitrary air filling fraction and refractive index contrast, a full vector formulation is required. A full vector FEM formulation based on anisotropic perfectly matched layers (PMLs) is able to calculate as many modes as desired in a single run without setting any iterative procedure (Saitoh and Koshiba 2001; Koshiba and Saitoh 2001).

2.1 Implementation of FEM on PCFs

The full – vectorial wave equation can be derived from Maxwell's equations for an optical waveguide with an arbitrary cross section as (Koshiba 1992):

$$\nabla \times \left([p] \nabla \times \phi \right) - k_0^2 [q] \phi = 0 \tag{1}$$

where ϕ represents the electric **E** or magnetic **H** field. The relative permittivity and permeability tensors [p] and [q] can be written as (Koshiba 1992);

$$[p] = \begin{bmatrix} p_x & 0 & 0 \\ 0 & p_y & 0 \\ 0 & 0 & p_z \end{bmatrix} \tag{2}$$

$$[q] = \begin{bmatrix} q_x & 0 & 0 \\ 0 & q_y & 0 \\ 0 & 0 & q_z \end{bmatrix} \tag{3}$$

where $p_x = p_y = p_z = 1$, $q_x = n_x^2$, $q_y = n_y^2$, $q_z = n_z^2$ for electric field (ϕ = E) and $q_x = q_y = q_z = 1$, $p_x = \frac{1}{n_x^2}$, $p_y = \frac{1}{n_y^2}$, $p_z = \frac{1}{n_z^2}$ for magnetic field ($\phi = \mathrm{H}$). In the above expressions, n_x, n_y and n_x represent the refractive indices in the x, y and z directions respectively.

2.2 Analysis of FEM with anisotropic PML

Technically, a PML is not a boundary condition but an additional domain that absorbs the incident radiation without producing reflections. It can have arbitrary thickness and is specified to be made of an artificial absorbing material. The material has anisotropic

permittivity and permeability that matches that of the physical medium outside the PML in such a way that there are no reflections regardless of the angle of incidence, polarisation and frequency of the incoming electromagnetic radiation (Koshiba and Saitoh 2001; Buksas 2001). The PML formulation can be deduced from Maxwell's equations by introducing a complex-valued coordinate transformation under the additional requirement that the wave impedance should remain unaffected (Buksas 2001).

If one considers a PML which is parallel to one of the Cartesian coordinate planes, an s matrix of the form (Koshiba 1992; Koshiba and Saitoh 2001):

$$[s] = \begin{bmatrix} \frac{s_y s_z}{s_x} & 0 & 0 \\ 0 & \frac{s_x s_z}{s_y} & 0 \\ 0 & 0 & \frac{s_x s_y}{s_z} \end{bmatrix} \tag{4}$$

$$[s]^{-1} = \begin{bmatrix} \frac{s_x}{s_y s_z} & 0 & 0 \\ 0 & \frac{s_y}{s_x s_z} & 0 \\ 0 & 0 & \frac{s_z}{s_x s_y} \end{bmatrix} \tag{5}$$

can be substituted into Eqn. (1) to permit the use of anisotropic PML. The modified equation thus becomes;

$$\nabla \times \left([p][s]^{-1} \nabla \times \phi \right) - k_0^2 [q][s]\phi = 0 \tag{6}$$

The parameters s_x, s_y, and s_z are complex valued scaling parameters. These parameters are set to α (α = 1 – α_j for leaky mode analysis), when we want to absorb the travelling wave in that direction and unity when no absorption is need. Thus, the absorption by the PML can be controlled by appropriate choice of α_j. A parabolic profile is assumed for α_j such that:

$$\alpha_j = \alpha_{j\max} \left(\frac{\rho}{\omega} \right)^2 \tag{7}$$

where ρ is the distance from the beginning of the PML and ω, the thickness of the PML.

3. Sensor design and numerical modelling

The proposed PCF SPR biosensor (Fig. 1) consists of circular air holes arranged in a hexagonal lattice, with a small circular air hole at the center. The air hole to air hole spacing is denoted by Λ, whilst d_2 represents the diameters of the circular air holes in the first ring.

Extra air holes of diameter d_{01} are inserted between the main air holes as a means of reducing the propagation losses whilst ensuring efficient coupling between the core guided and plasma modes. A small air hole of diameter d_1 is introduced into the core to facilitate phase matching with a plasmon by lowering the refractive index of the core-guided mode. The first layer of holes work as a low refractive index cladding, enabling mode guidance in the fiber core. The second ring has two slots of uniform thickness d_3, which houses the analyte. Theses slots are coated with gold of thickness t_{Au}. The gap between slots is set to be equal to d_2 throughout this study.

The background material is made of silica which is modeled using the Sellmeier equation (Sellmeier 1871);

$$n(\lambda) = \sqrt{1 + \frac{B_1\lambda^2}{\lambda^2 - C_1} + \frac{B_2\lambda^2}{\lambda^2 - C_2} + \frac{B_3\lambda^2}{\lambda^2 - C_3}} \tag{8}$$

where n is the refractive index, λ , the wavelength in μm, B(i = 1,2,3) and C(i = 1,2,3) are Sellmeier coefficients. The Sellmeier coefficients used for the background material are B_1=0.696166300, B_2=0.407942600, B_3=0.897479400, C_1=4.67914826×10^{-3}μm^2, C_2=1.35120631×10^{-2} μm^2 and C_3= 97.9340025 μm^2 (Sellmeier 1871). The permittivity of gold and silver is modeled using data from Johnson and Christy(Johnson and Christy 1972).

Simulations were carried out using a full-vectorial finite element method (FEM) with perfectly matched layers (PMLs). The cross section of the proposed PCF SPR biosensor is divided into many sub-domains with triangular shaped elements in such a way that the step index profiles can be exactly represented. Due to the symmetrical nature of the PCF structure, only one-quarter of the sensor cross section is divided into curvilinear hybrid elements. This results in a computational window area of (5 μm × 5 μm) terminated by a PML of width = 1 μm. The mesh size is 19,062 elements. Modal analysis of the fundamental mode has been performed on the cross section in the x-y plane of the PCF as the wave is propagating in the z – direction.

4. Simulation results

We begin our analysis by investigating the potential of the proposed PCF for sensing. The structural parameters used are Λ = 1.5 μm, d_1/Λ= 0.2, d_2/Λ= 0.35, d_{01}/Λ = 0.15, d_3= 1.5 μm and t_{Au} = 40 nm. The slots in the second ring are first filled with an analyte whose refractive index, n_a = 1.33 (water) after which the confinement loss of the fundamental mode is calculated. The process is repeated with an analyte of refractive index of 1.34 and the calculated loss spectra for both cases are plotted in Fig 2. It can be observed from Fig. 2 that there are two major attenuation peaks which correspond to the excitation of plasmonic modes on the surface of the metalized channels filled with aqueous analyte , n_a=1.33. It is important to note that the shape of a metallized surface can have a significant effect on the plasmonic excitation spectrum. Hence, a planar metallized surface supports only one plasmonic peak, while a cylindrical metal layer can support several plasmonic peaks.

By changing the analyte refractive index from 1.33 to 1.34, it is observed in Fig. 2 that there is a corresponding shift (dashed curves) in the resonant attenuation peaks. This transduction mechanism is commonly used for detecting the bulk analyte refractive index changes, as

well as monitoring formation of the nanometer-thin biolayers on top of a metallized sensor surface (Hassani and Skorobogatiy 2006). In this particular design, there is considerably more field penetration into the analyte-filled channels for the first plasmonic peak as compared to that of the second. This makes it more sensitive than the second with regards to analyte refractive index changes. All subsequent analysis will be based on the first plasmonic peak as it is the most sensitive to refractive index change.

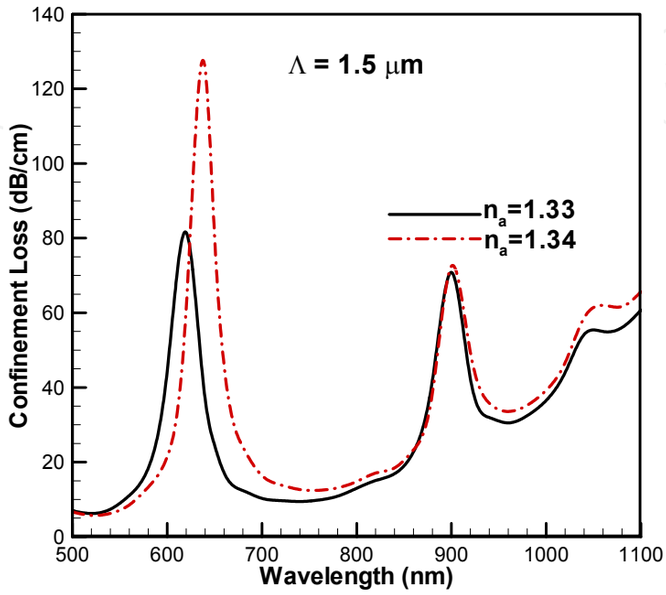

Fig. 2. Calculated loss spectra of the fundamental modes. Loss spectra (solid curves) feature several attenuation peaks corresponding to the excitation of plasmonic modes on the surface of metallized channels filled with aqueous analyte (n_a = 1.33). A change in analyte refractive index (dashed curves) leads to a corresponding shift in the points of phase matching between the core-guided and plasmon modes.

4.1 Optimisation of structural parameters

In order to optimise the several structural parameters of the proposed PCF SPR biosensor for high spectral sensitivity, it is important to understand the effects these parameters have on the sensor properties. Surface plasmon waves, being surface excitations, are very sensitive to the thickness of metallic layers. We therefore investigate the changes in the spectra for the first plasmonic peak when the thickness of gold t_{Au}, is varied from 30 nm to 50 nm. The analyte in this case is fixed at a refractive index of 1.33 and all other structural parameters are kept constant. The confinement loss for the fundamental mode is calculated for each case of t_{Au} and plotted to give the spectra in Fig. 3.

Figure 3 shows a general decrease in modal propagation loss at resonance when the thickness of the gold layer increases. In addition, there is a shift in the resonant wavelength towards longer wavelengths for every increase in t_{Au}. Specifically, the resonant wavelength shifts from about 580 nm to 640 nm for t_{Au} values of 30 nm and 50 nm respectively. This sensitivity of the resonant wavelength to the gold thickness can be used in the study of metal nanoparticle binding events on the metallic surface of the sensor (Hassani and

Skorobogatiy 2006). Practically, this can be used in the monitoring of concentration of metal nanoparticles attached to the photosensitive drugs in photodynamic cancer therapy (Hassani and Skorobogatiy 2006).

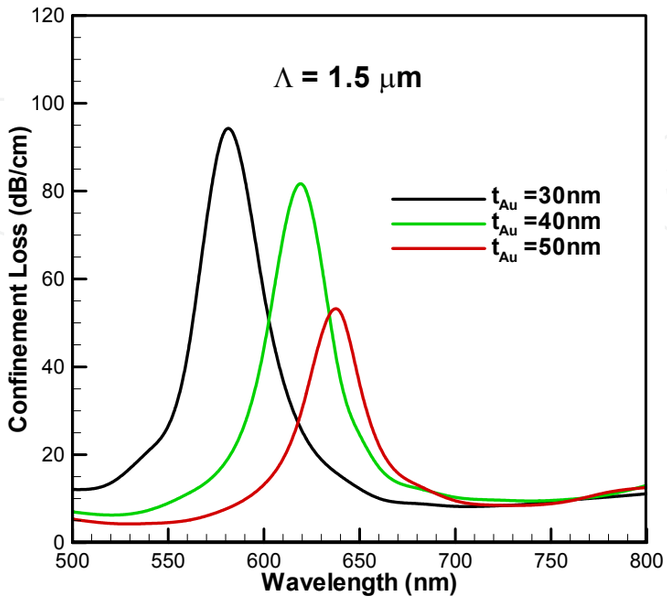

Fig. 3. Loss spectra of proposed PCF SPR biosensor in the vicinity of the first plasmonic peak for variation in gold layer thickness (t_{Au}). Analyte refractive index (na=1.33), $d_{01}/\Lambda = 0.15$, $d_1/\Lambda = 0.2$, $d_2/\Lambda = 0.35$.

In this particular design, a central air hole of diameter d_1, has been employed to tune the phase matching condition. In what follows, we investigate the effect of size variation of the central air hole, with a view of tuning and optimizing plasmon excitation by the core-guided mode of the proposed PCF SPR biosensor. In order to achieve this, d_1/Λ is varied from 0.15 to 0.25 whilst keeping all other structural parameters constant. The micro-fluidics slots are filled with analyte of refractive index, n_a = 1.33 for each calculation of the loss spectra for every change in the value of d_1/Λ. Figure 4 shows that there is an overall increase in the modal losses of the fundamental mode for the larger diameters of the central air hole. An increase in the size of the central air hole promotes expulsion of the modal field from the fiber core. This in turn, leads to the greater modal presence near the metallic interface, resulting in higher propagation losses.

Another consequence of the modal expansion from the fiber core into the air-filled microstructure is reduction of the modal refractive index (Fig. 5), leading to the shift of a plasmonic peak toward longer wavelengths (Fig. 4).

In particular, the resonant wavelength changes from about 615 nm to 620 nm for d_1/Λ values of 0.15 and 0.25 respectively.

The next step of the analysis focuses on the influence of the extra air holes, d_{01}, on the confinement loss and resonant wavelength of the PCF SPR sensor. To achieve this, d_{01}/Λ is varied from 0.10 to 0.20, whilst keeping all other structural parameters constant. The micro-fluidics slots are filled with analyte of refractive index, n_a = 1.33 for each computation of the

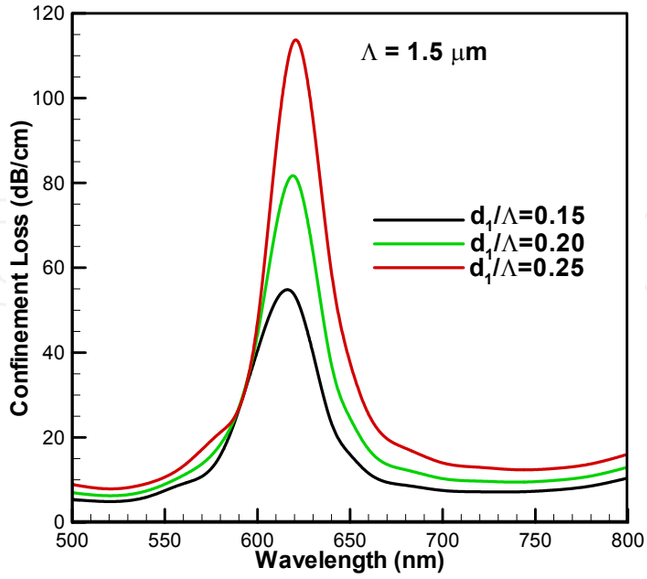

Fig. 4. Loss spectra of proposed PCF SPR biosensor in the vicinity of the first plasmonic peak for variation in d_1. Analyte refractive index (n_a=1.33), d_{01}/Λ = 0.15, t_{Au} = 40 nm, d_2/Λ = 0.35.

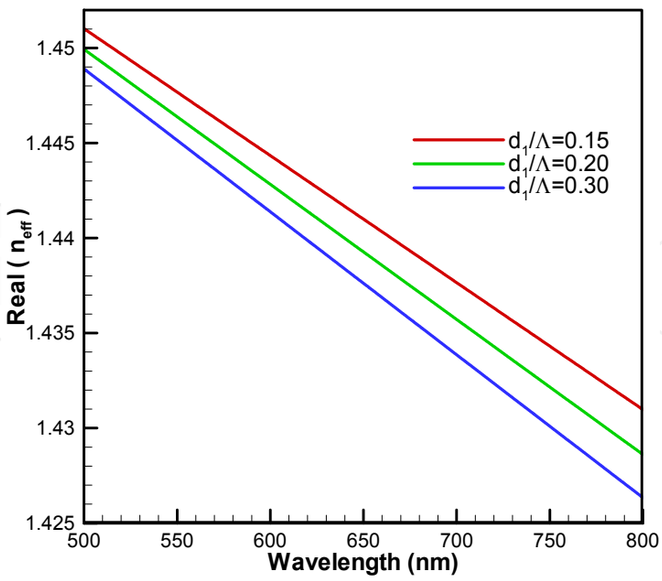

Fig. 5. Dispersion relation of the fundamental mode for variation in d_1. Analyte refractive index (n_a=1.33), d_{01}/Λ = 0.15, t_{Au} = 40 nm, d_2/Λ = 0.35.

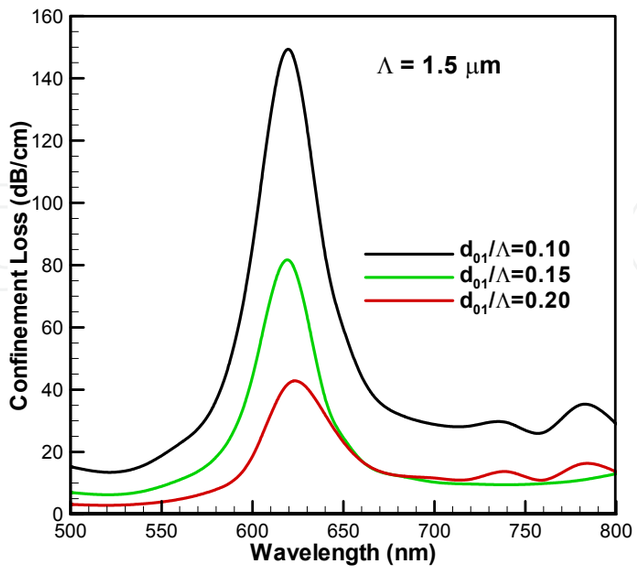

Fig. 6. Loss spectra of proposed PCF SPR biosensor in the vicinity of the first plasmonic peak for variation in d_{01}. Analyte refractive index (n_a=1.33), t_{Au} = 40 nm, d_1/Λ = 0.20, d_2/Λ = 0.35.

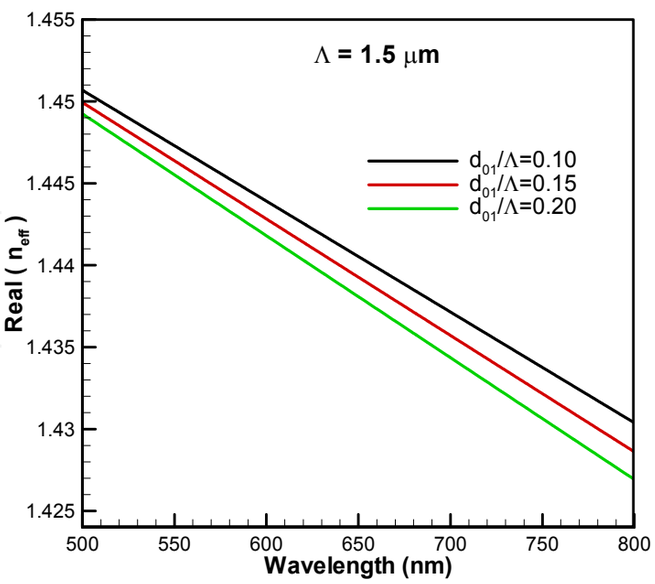

Fig. 7. Dispersion relation of the fundamental mode for variation in d_{01}. Analyte refractive index (na=1.33), t_{Au} = 40 nm, d_1/Λ = 0.20, d_2/Λ = 0.35.

loss spectra for a change in the value of d_{01}/Λ. Figure 6 shows that the extra air holes could be used to play a significant role in confinement loss reduction. Unlike d_1, increasing d_{01} reduces the confinement loss whilst shifting the resonant wavelength towards longer wavelength. However, d_{01} has less influence on the resonant wavelength as compared to d_1 and can be considered as a loss control parameter. An increase in d_{01} prevents expulsion of the modal field from the fibre core, thus ensuring better confinement to the core. This ultimately reduces the confinement loss at the resonant wavelength. The decrease in the modal effective index (Fig. 7) for an increase d_{01}/Λ is due to the fact that the "escaping" mode field from the core interacts with relatively larger air filled spaces.

4.1.1 Characterization of sensitivity of the proposed PCF SPR biosensor

The detection of changes in the bulk refractive index of an analyte is the simplest mode of operation of fibre - based SPR biosensors (Hassani and Skorobogatiy 2006; Piliarik, Párová, and Homola 2009; Homola 2003). There is a strong dependence of the real part of a plasmon refractive index on the analyte refractive index, which makes the wavelength of phase matching between the core-guided and plasmon modes sensitive to the changes in the analyte refractive index (Homola 2003; Piliarik, Párová, and Homola 2009). Amplitude (phase) and wavelength interrogation are two main detection methods (Homola 2003; Piliarik, Párová, and Homola 2009).

In the amplitude or phase based method, all measurements are done at a single wavelength (Homola 2003). This approach has the merit of its simplicity and low cost as there is no spectral manipulation needed (Homola 2003). The disadvantage however, is that a smaller operational range and lower sensitivity when compared with the wavelength interrogation methods, where the transmission spectra are taken and compared before and after a change in in analyte refractive index has occurred(Homola 2003).

The amplitude sensitivity is given by(Hassani and Skorobogatiy 2006):

$$S_A(\lambda) = -(\partial\alpha(\lambda, n_a) / \partial n_a) / \alpha(\lambda, n_a) \ [\text{RIU}^{-1}] \tag{9}$$

where $\alpha(\lambda, n_a)$ represents the propagation loss of the core mode as a function of wavelength.

When the sensor operates in the wavelength interrogation mode, changes in the analyte refractive index are detected by measuring the displacement of a plasmonic peak. The sensitivity in this case is given by (Hassani et al. 2008; Homola 2003):

$$S_\lambda(\lambda) = \frac{\partial \lambda_{peak}}{\partial n_a} \ [\text{nm / RIU}] \tag{10}$$

where λ_{peak} is the wavelength corresponding to the resonance (peak loss) condition. The proposed SPR sensor operates in wavelength interrogation mode. Thus all sensitivity analysis will be limited to spectral interrogation.

It can be observed from Fig. 8 that the thickness of the gold layer (t_{Au}) in the microfluidic slots has an influence on the shift in resonant wavelength. Specifically, the change in resonant wavelength (λ_{peak}) is inversely proportional to t_{Au}. This is due to the fact that when

the thickness of the gold layer becomes significantly larger than that of its skin depth, (~20–30 nm), the fibre core mode becomes effectively screened from a plasmon, resulting in a low coupling efficiency, culminating in low sensitivity. Hence, the maximum shift of 20 nm occurs for t_{Au} of 30 nm (Fig. 8). This results in a maximum sensitivity of 2000 nm/RIU according to Eqn. (9).

The next step involves investigating the influence of d_1 on the spectral sensitivity of the PCF SPR sensor under consideration. It can be observed from Fig. 9 that the effect of d_1 on the spectral sensitivity follows the same trend as that of t_{Au}. Specifically, the sensitivity increases with d_1/Λ to a maximum of approximately 2100 nm / RIU for d_1/Λ value of 0.25. An increase in d_1/Λ ensures more leakage of the fundamental mode into the metal / analyte layer in the microfluidic slots, resulting in greater sensitivity of analyte refractive index change.

5. An optimised structure for higher spectral sensitivity

The analysis done so far gives some insight into the effects the structural parameters have on sensor performance. These results are summarised in Table 1.

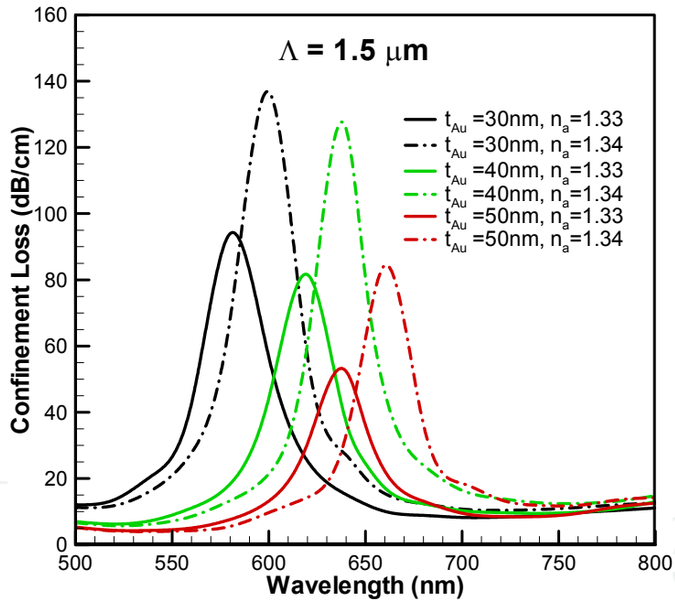

Fig. 8. Shift in resonant wavelength of the loss spectrum for a variation in tAu of the proposed SPR sensor. Analyte refractive index (n_a =1.33), d_{01}/Λ = 0.15, d_1/Λ = 0.2, d_2/Λ = 0.35.

According to Table 1, d_{01}, t_{Au} and d_1 can be considered as loss control parameters. With regards to spectral sensitivity, the main candidates to consider are t_{Au} and d_1. Of these two parameters, d_1 appears relatively easier to control as compared to t_{Au}. It will therefore be more convenient to fix t_{Au} to an appropriate value and optimise d_1 to achieve the desired sensitivity. It must also be noted that there is a limit to which d_1 can be increased due to the associated high confinement losses. To minimise the confinement losses, d_{01} can optimised

to keep much of the field inside the core without compromising much sensitivity. By taking all these factors into consideration, the final set of device parameters to maximise sensitivity whilst maintaining an appreciable confinement loss are; Λ = 1.5 μm, d_1/Λ = 0.50, d_{01}/Λ = 0.20, t_{Au} = 40 nm.

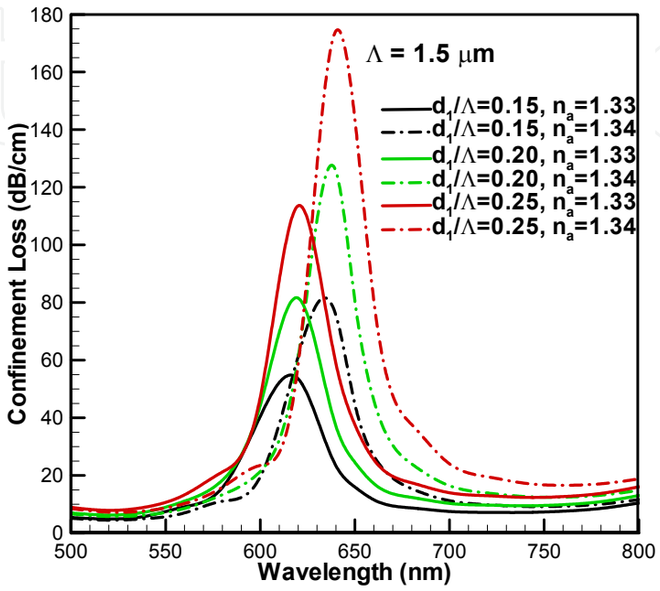

Fig. 9. Shift in resonant wavelength of the loss spectrum for a variation in d_1 of the proposed SPR sensor. Analyte refractive index (n_a=1.33), d_{01}/Λ = 0.15, t_{Au} = 40 nm, d_2/Λ = 0.35.

Parameter	Sensitivity $S_\lambda(\lambda)$	Resonant Wavelength (λ_{peak})	Confinement Loss
d_1↑	↑	↑	↑
d_{01}↑	↑ - But has less influence on it due to the fact that there is a relatively small change in λ_{peak} for a slight increase in d_{01}.	↑ - But it has less influence on it as compared to t_{Au} and d_1.	↓
t_{Au}↑	↑	↑	↓

Table 1. Summary of influence of structural parameters on properties of the proposed PCF SPR biosensor.↑ represents an increase in a parameter or property whilst ↓ represents a decrease.

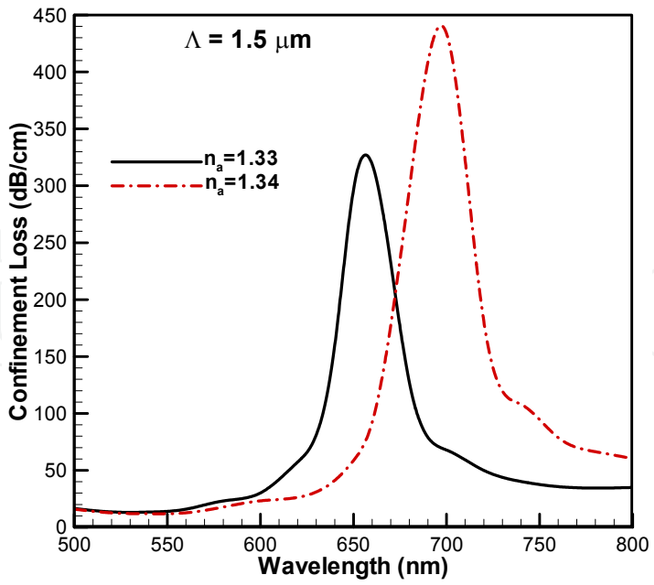

Fig. 10. Shift in resonant wavelength of the optimised PCF SPR biosensor. Structural parameters; Λ = 1.5 μm, d_1/Λ = 0.50, d_{01}/Λ = 0.20, t_{Au} = 40 nm.

Figure 10 shows the shift in resonant wavelength for a change in analyte refractive index from n_a = 1.33 to n_a = 1.34 for the optimised structure. It indicates an improvement in the spectral sensitivity, which is now approximately 4000 nm / RIU. If the assumption is made that 0.1nm change in the position of a resonance peak can be detected reliably, the resulting sensor resolution is 2.5×10^{-5} RIU, which is better than the 3×10^{-5} RIU and 1×10^{-4} RIU reported by (Hassani and Skorobogatiy 2006) and (Hautakorpi, Mattinen, and Ludvigsen 2008)respectively. The optimisation procedure presented so far can give an indication of the manufacturing tolerances acceptable, to maintain the estimated sensor sensitivity. Of particular interest is the fabrication tolerance of the air holes of the PCF SPR sensor structure. It can be concluded from Fig. 6, 9 and 10 that the maximum allowable change in both d_{01}/Λ and d_1/Λ to maintain the estimated sensitivities, is 50%. Hence, the proposed design can maintain its estimated sensitivity of 4000 nm / RIU provided the holes are fabricated within the 50% tolerance assuming all other conditions remain constant. The current state of advanced PCF fabrication technologies, make fabrication within this tolerance possible.

Since sensor length is inversely proportional to the modal loss, optimization of the PCF structural parameters allows design of PCF SPR sensors of widely different lengths (from millimetre to meter), while having comparable sensitivities. Due to the relatively high loss of our proposed PCF SPR sensor, its length is limited to the centimetre scale. Therefore, the proposed sensor should be rather considered as an integrated photonics element than a fibre.

6. Conclusion

The design and optimisation of a novel PCF SPR biosensor has been presented in this chapter. The loss spectra, phase matching conditions and sensitivity of the proposed biosensor have been presented using a full – vector FEM with PML.

It has been shown that the proposed PCF SPR sensor can be optimised to achieve a sensitivity of 4000 nm/RIU with regards to spectral interrogation, which is much higher than the 1000 nm/RIU and 3000 nm/RIU reported by (Hassani and Skorobogatiy 2006) and (Hautakorpi, Mattinen, and Ludvigsen 2008) respectively. In addition, the PCF SPR sensor incorporates the micro-fluidics setup, waveguide and metallic layers into a single structure. This makes the proposed design compact and more amenable to integration as compared to conventional fibre SPR biosensors.

With regards to fabrication, the proposed structure should be relatively easy to fabricate due to the notably large micro fluidic slots. Deposition of metal layers inside of the micro fluidic slots can be performed either with the high-pressure chemical vapor deposition technique (Sazio 2006) or electroless plating techniques used in fabrication of metalized hollow waveguides and microstructures (Harrington 2000; Takeyasu, Tanaka, and Kawata 2005).

7. References

Ademgil, H., S. Haxha, T. Gorman, and F. AbdelMalek. 2009. Bending Effects on Highly Birefringent Photonic Crystal Fibers With Low Chromatic Dispersion and Low Confinement Losses. *Journal of Lightwave Technology* 27 (5-8):559-567.

Akowuah, E. K., T. Gorman, S. Haxha, and J. V. Oliver. 2010. Dual channel planar waveguide surface plasmon resonance biosensor for an aqueous environment. *Optics Express* 18 (24):24412-24422.

Buksas, M. W. 2001. Implementing the perfectly matched layer absorbing boundary condition with mimetic differencing schemes - Abstract. *Journal of Electromagnetic Waves and Applications* 15 (2):201-202.

Dhawan, Anuj, Michael D. Gerhold, and John F. Muth. 2008. Plasmonic structures based on subwavelength apertures for chemical and biological sensing applications. *Ieee Sensors Journal* 8 (5-6):942-950.

Ferrando, A., E. Silvestre, J. J. Miret, P. Andres, and M. V. Andres. 2000. Vector description of higher-order modes in photonic crystal fibers. *Journal of the Optical Society of America a-Optics Image Science and Vision* 17 (7):1333-1340.

Gauvreau, Bertrand, Alireza Hassani, Majid Fassi Fehri, Andrei Kabashin, and Maksim Skorobogatiy. 2007. Photonic bandgap fiber-based surface plasmon resonance sensors. *Optics Express* 15 (18):11413-11426.

Harrington, J. A. 2000. A review of IR transmitting, hollow waveguides. *Fiber and Integrated Optics* 19 (3):211-227.

Hassani, A., B. Gauvreau, M. F. Fehri, A. Kabashin, and M. Skorobogatiy. 2008. Photonic crystal fiber and waveguide-based surface plasmon resonance sensors for application in the visible and Near-IR. *Electromagnetics* 28 (3):16.

Hassani, A., and M. Skorobogatiy. 2006. Design of the microstructured optical fiber-based surface plasmon resonance sensors with enhanced microfluidics. *Optics Express* 14 (24):11616-11621.

Hautakorpi, Markus, Maija Mattinen, and Hanne Ludvigsen. 2008. Surface-plasmon-resonance sensor based on three-hole microstructured optical fiber. *Optics Express* 16 (12):8427-8432.

Hoa, X. D., A. G. Kirk, and M. Tabrizian. 2007. Towards integrated and sensitive surface plasmon resonance biosensors: A review of recent progress. *Biosensors & Bioelectronics* 23 (2):151-160.

Homola, Jirí, Sinclair S. Yee, and Günter Gauglitz. 1999. Surface plasmon resonance sensors: review. *Sensors and Actuators B: Chemical* 54 (1-2):3-15.

Homola, Jiří. 2003. Present and future of surface plasmon resonance biosensors. *Analytical and Bioanalytical Chemistry* 377 (3):528-539.

Jha, R., and A. K. Sharma. 2009. High-performance sensor based on surface plasmon resonance with chalcogenide prism and aluminum for detection in infrared. *Optics Letters* 34 (6):749-751.

Johnson, P. B., and R. W. Christy. 1972. Optical - Constants of Noble-Metals. *Physical Review B* 6 (12):4370-4379.

Jorgenson, R.C., and S.S. Yee. 1993. A fiber-optics chemical sensor based on surface plasmon resonance. *Sens. Actuators B* 12:213–220.

Koshiba, M. 1992. *Optical Waveguide Theory by the Finite Element Method*: KTK Scientific Publishers.

Koshiba, M., and K. Saitoh. 2001. Numerical verification of degeneracy in hexagonal photonic crystal fibers. *Ieee Photonics Technology Letters* 13 (12):1313-1315.

Monzon-Hernandez, D., and J. Villatoro. 2006. High-resolution refractive index sensing by means of a multiple-peak surface plasmon resonance optical fiber sensor. *Sensors and Actuators B-Chemical* 115 (1):227-231.

Mouvet, C., R. D. Harris, C. Maciag, B. J. Luff, J. S. Wilkinson, J. Piehler, A. Brecht, G. Gauglitz, R. Abuknesha, and G. Ismail. 1997. Determination of simazine in water samples by waveguide surface plasmon resonance. *Analytica Chimica Acta* 338 (1-2):109-117.

Nooke, A., U. Beck, A. Hertwig, A. Krause, H. Krueger, V. Lohse, D. Negendank, and J. Steinbach. 2010. On the application of gold based SPR sensors for the detection of hazardous gases. *Sensors and Actuators B-Chemical* 149 (1):194-198.

Patskovsky, S., M. Meunier, P. N. Prasad, and A. V. Kabashin. 2010. Self-noise-filtering phase-sensitive surface plasmon resonance biosensing. *Optics Express* 18 (14):14353-14358.

Piliarik, Marek, Lucie Párová, and Jirí Homola. 2009. High-throughput SPR sensor for food safety. *Biosensors and Bioelectronics* 24 (5):1399-1404.

Piliarik, Marek, Milan Vala, Ivo Tichý, and Jirí Homola. 2009. Compact and low-cost biosensor based on novel approach to spectroscopy of surface plasmons. *Biosensors and Bioelectronics* 24 (12):3430-3435.

Saitoh, K., and M. Koshiba. 2001. Full-vectorial finite element beam propagation method with perfectly matched layers for anisotropic optical waveguides. *Journal of Lightwave Technology* 19 (3):405-413.

Sazio, P J A. 2006. Microstructured optical fibers as highpressure microfluidic reactors. *Science* 311:1583-1586.

Sellmeier, W. 1871. Zur Erklärung der abnormen Farbenfolge im Spectrum einiger Substanzen. *Ann. Phys. Chem* 6 (219):272–282.

Takeyasu, N., T. Tanaka, and S. Kawata. 2005. Metal deposition deep into microstructure by electroless plating. *Japanese Journal of Applied Physics Part 2-Letters & Express Letters* 44 (33-36):L1134-L1137.

Wang, K., Z. Zheng, Y. L. Su, Y. M. Wang, Z. Y. Wang, L. S. Song, J. Diamond, and J. S. Zhu. 2010. High-Sensitivity Electro-Optic-Modulated Surface Plasmon Resonance Measurement Using Multilayer Waveguide-Coupled Surface Plasmon Resonance Sensors. *Sensor Letters* 8 (2):370-374.

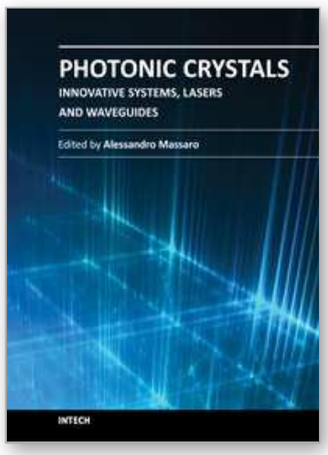

Photonic Crystals - Innovative Systems, Lasers and Waveguides

Edited by Dr. Alessandro Massaro

ISBN 978-953-51-0416-2
Hard cover, 348 pages
Publisher InTech
Published online 30, March, 2012
Published in print edition March, 2012

The second volume of the book concerns the characterization approach of photonic crystals, photonic crystal lasers, photonic crystal waveguides and plasmonics including the introduction of innovative systems and materials. Photonic crystal materials promises to enable all-optical computer circuits and could also be used to make ultra low-power light sources. Researchers have studied lasers from microscopic cavities in photonic crystals that act as reflectors to intensify the collisions between photons and atoms that lead to lazing, but these lasers have been optically-pumped, meaning they are driven by other lasers. Moreover, the physical principles behind the phenomenon of slow light in photonic crystal waveguides, as well as their practical limitations, are discussed. This includes the nature of slow light propagation, its bandwidth limitation, coupling of modes and particular kind terminating photonic crystals with metal surfaces allowing to propagate in surface plasmon-polariton waves. The goal of the second volume is to provide an overview about the listed issues.

INTECH
open science | open minds

InTech Europe
University Campus STeP Ri
Slavka Krautzeka 83/A
51000 Rijeka, Croatia
Phone: +385 (51) 770 447
Fax: +385 (51) 686 166
www.intechopen.com

InTech China
Unit 405, Office Block, Hotel Equatorial Shanghai
No.65, Yan An Road (West), Shanghai, 200040, China
中国上海市延安西路65号上海国际贵都大饭店办公楼405单元
Phone: +86-21-62489820
Fax: +86-21-62489821

IntechOpen